Hindawi
International Journal of Aerospace Engineering
Volume 2024, Article ID 5557153, 17 pages
https://doi.org/10.1155/2024/5557153

Research Article

Multidisciplinary Design Optimization of Reentry-Powered Hypersonic Vehicles Based on Surrogate Model

Shoudong Ma, Yuxin Yang, Yesi Chen, Hua Yang, and Weifang Chen

School of Aeronautics and Astronautics, Zhejiang University, Hangzhou 310027, China

Correspondence should be addressed to Hua Yang; yhsaa@zju.edu.cn

Received 13 December 2023; Revised 12 March 2024; Accepted 21 March 2024; Published 20 April 2024

Academic Editor: Tuo Han

Two problems exist in the study of the trajectory optimization problem of powered hypersonic gliding vehicles (HGVs) due to insufficient consideration of the overall design constraints as well as the strong couplings among relevant disciplines: (1) the engine and thrust models are not compatible with the existing HGV; (2) configuration parameters of the HGV are not included as design variables during trajectory optimization (i.e., propulsion discipline is decoupled in the process of the HGV configuration design), thus failing to fully explore the effect of power to improve the performance of the HGV. Therefore, the application of multidisciplinary design optimization (MDO) in the overall design of powered HGVs should be investigated. First, a MDO task analysis and a multidisciplinary model analysis are carried out for the powered HGV. Second, the multidisciplinary optimization problem is defined, and the couplings between disciplines of the powered HGV are analyzed so that a six-discipline model is established that is suitable for the overall design process, including the parameterized configuration geometry, aerodynamics, propulsion, mass properties, trajectory, and aerodynamic heat/thermal protection system (TPS). Finally, a surrogate model is used to replace the time-consuming accurate model, and numerical optimization examples verify the effectiveness of the method. The optimization results show that the method has a good convergence speed, which increases the gliding range of the optimized vehicle by 8.37%. In addition, by decoupling the propulsion discipline, the validation shows that the coupled propulsion discipline during the overall design can increase the range of the powered HGV by 3.87% compared to the powered HGV optimized with the decoupled propulsion discipline. The work done in this paper provides a new design idea for the overall design of a powered HGV.

Keywords: multidisciplinary design optimization; powered hypersonic glide vehicle; surrogate model

1. Introduction

Hypersonic gliding vehicles (HGVs) generally refer to near-space vehicles with flight speeds greater than Mach 5 [1, 2]. Because of its extremely high flight speed, large span of flight airspace, and strong maneuverability, it is increasingly valued by spacefaring powers [3–5]. Compared with traditional ballistic missiles, hypersonic glide vehicles have the advantages of strong mobility, flexible and variable trajectory, and difficulty intercepting. They are essential weapons and equipment for future near-space combat, breakthrough anti-missile defense systems, intercept ballistic missiles, and rapid global strikes. They have a wide range of application prospects in the military [6–8].

However, traditional HGVs are unpowered, with limited maneuverability during reentry and range loss after maneuvering, which makes it impossible to complete the established tasks [9–11]. To improve the range and maneuverability of HGVs, relevant scholars have proposed the method of carrying engines for power augmentation, and the trajectory optimization problem of such vehicles with engine power augmentation has been studied. Luo et al. [12] proposed a trajectory optimization design method based on hybrid control of aerodynamic forces and rocket engine thrust, which utilizes the strategy of replenishing kinetic energy once or twice during vehicle glide reentry to achieve a significant increase in the range of the vehicle. Lin, He, and Huang [13, 14] studied the trajectory optimization problem of

HGVs with discontinuous ignition. They improved the range of the vehicle by reasonably setting the ignition moment and the number of ignition times. Chai et al. [15] used the Gaussian pseudospectral method to optimize the trajectory of an aspirating cruise missile and used an intermittent ignition scheme to obtain the hopping trajectory at different altitudes, effectively improving the vehicle's maneuverability. Feng et al. [16] realized the "floating" trajectory through simulation under the conditions of stratified atmospheric density, suitable trajectory inclination, and sufficient fuel, which improved the breakout capability and ensured the optimal range. Lin, He, and Wang [17] investigated the effects of the parameters of the powered vehicle ignition time, ignition phase duration, and tilt angle profile on the maneuverability and range of the vehicle. The results show that different power supplementation strategies affect vehicle performance differently. However, in general, supplemental power can still improve the overall performance of vehicles. The research of the above scholars can fully prove that the reentry-powered hypersonic vehicle has better endurance and maneuverability than the traditional vehicle.

However, the overall design constraints of the powered HGV and the multidisciplinary coupling relationships were not fully considered in the above studies, and the conclusions need to be revised. First, none of the trajectory optimization phases considered the adaptability of the engine model to the overall design. The thrust model is simplified, which may make the hypothetical engine and thrust model unable to meet the general requirements of the vehicle and thus unable to demonstrate the effectiveness of improving the vehicle performance under that engine and thrust model. Second, the trajectory optimization phase does not incorporate the configuration parameters of the vehicle into the optimization variables, that is, it does not take into account the coupling between the geometric attributes of the vehicle and the propulsion, trajectory, and other disciplines and is unable to exploit the role of power for vehicle performance enhancement adequately. In summary, the coupling effect between disciplines should be fully considered from the overall design perspective to enhance the performance of powered HGVs. Some scholars [18, 19] have used parametric modeling methods to study the optimization process of HGVs in the conceptual design stage and scheme formation stage, and the results show that the overall design optimization of HGVs is a complex nonlinear optimization problem with serious multidisciplinary coupling and high computational resource requirements. The traditional serial design method can no longer better exploit the overall performance design potential. New design concepts and ideas must be introduced to improve the overall design process. The idea of multidisciplinary design optimization (MDO) was first proposed by Sobieszczanski-Sobieski [20] in 1982 and was first applied in the aerospace field with promising results [21, 22]. Viviani et al. [23] investigated the shape design of a reusable reentry vehicle using a multidisciplinary optimization design method and combining it with computational fluid dynamics (CFD), obtaining a vehicle shape that meets the mission requirements and reduces the cost of commercial launches. Yan and Zhang [24] established a multidisciplinary optimal design methodology based on a multidisciplinary design feasible (MDF) architecture and simplified it according to specific designs. A simplified version of the NSGA-II algorithm with an adaptive active control strategy was proposed to solve the problem of highly complex startup safety assessment due to the tightly coupled design parameters and limited objectives. Benaouali and Kachel [25] investigated the optimization problem of an airfoil by establishing a multidisciplinary optimization methodology integrating commercial software. Instead of high-cost numerical simulation, an agent-based modeling optimization strategy was used, and the optimized airfoil could improve the reachability domain of the aircraft by 8.3%. Zhang, Tang, and Che [26] established a multidisciplinary performance analysis model targeting vehicles similar to X-43A involving parametric configuration geometry, aerodynamics, propulsion, aerodynamic thermals, mass properties, radar cross section (RCS), and trajectory and used a parallel subspace optimization method for the design optimization, based on the polynomial response surface approximation technique, to optimize the design. The range of the optimized vehicle is increased by 18.9%. The successful application of the multidisciplinary optimization design method in the overall design of many hypersonic vehicles demonstrates the method's reliability in solving the problems of severe coupling of various disciplines in the vehicle design process.

Powered HGVs have a better range and stronger maneuvering than unpowered HGVs. However, the existing research has not fully considered the overall design constraints and multidisciplinary couplings. There may be problems such as the engine cannot be adapted and cannot be fully tapped into the effect of the power on the vehicle performance enhancement. To address these issues, this paper applies an MDO approach to the overall design of powered HGVs. It systematically investigates various aspects, including multidisciplinary optimization task planning and requirements analysis, multidisciplinary modeling, system definition, design, system integration, and solving. A comparative analysis illustrates the importance of utilizing MDO methods in the overall design of powered HGVs and the necessity of working with multidisciplinary optimization design carrying out coupled propulsion disciplines. This study provides new design insights for the overall design of such vehicles. The article is organized as follows: Section 2 describes the multidisciplinary optimization task analysis, Section 3 presents the models of the various disciplines involved in the overall design, Section 4 defines the MDO problem, Section 5 illustrates the system integration and optimization methodology, Section 6 gives a case study of optimization of a powered vehicle, Section 7 provides a comparison of the optimization results of the coupled/decoupled propulsion disciplines, and Section 8 summarizes the whole paper.

2. Multidisciplinary Optimization Task Analysis

2.1. Baseline Scheme and Overall Design Features. The powered HGV studied in this paper is based on a vehicle similar to HTV-2 [27], as shown in Figure 1, and the aerodynamic layout is in the form of a lifting body. The vehicle glide

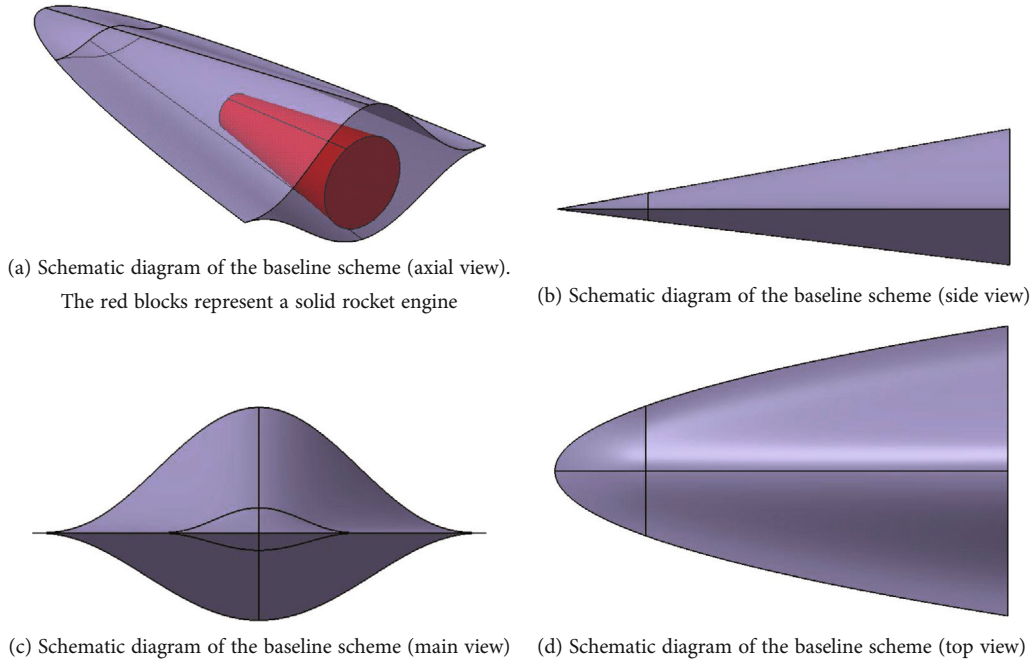

(a) Schematic diagram of the baseline scheme (axial view). The red blocks represent a solid rocket engine

(b) Schematic diagram of the baseline scheme (side view)

(c) Schematic diagram of the baseline scheme (main view)

(d) Schematic diagram of the baseline scheme (top view)

Figure 1: Schematic diagram of the baseline scheme.

reentry altitude is at least 80 km, and the maximum range is at least 15,000 km. During the gliding process, the solid rocket motor installed at the bottom makes up the energy to increase the range.

Compared with the traditional ballistic flight scheme, the HGV adopts the near-space maneuvering flight scheme, and the relationship between the various professional disciplines related to the overall performance has significantly changed. The coupling between the disciplines has become more prominent. Its overall design is characterized by the fact that the vehicle's maximum range is affected by two critical factors, namely, aerodynamic force characteristics and trajectory design, in addition to the thrust-to-weight ratio. Therefore, the overall design should emphasize the coupling between the propulsion, mass, configuration, and trajectory.

2.2. MDO Tasks. From the overall design characteristics of the powered HGV, its MDO process involves six professional disciplines: configuration, aerodynamics, mass, propulsion, trajectory, and aerodynamic heat/thermal protection system (TPS). The specific parameters of the baseline scheme are determined through repeated coordination calculations between disciplines, and the optimal overall plan is obtained using optimization algorithms. The task of the MDO of the powered HGV is to describe the above design process using appropriate mathematical models, determine the system decomposition and coordination strategy based on the couplings of the overall design, solve it through proper system integration and optimization algorithms, and fully tap the potential of the overall design of the powered gliding aircraft. According to the general design task, the disciplines and couplings are shown in Figure 2.

The functions of each module are as follows:

1. Configuration: describes the main geometric characteristics of the aircraft, provides geometric information to each discipline, and modifies geometric parameters based on variables assigned by the optimizer or feedback information from disciplines.

2. Aerodynamics: computes the aerodynamic performance within the flight envelope and provides data for trajectory calculations.

3. Propulsion: computes engine performance, provides data for trajectory calculations, and determines the engine mass.

4. Trajectory: calculates the flight trajectory of the powered HGV, evaluating its completed mission capabilities.

5. Mass: determines the overall mass of the HGV based on the geometric model, propulsion, TPS, and payload.

6. Aerodynamic heat/TPS: computes internal heat transfer within the structure, determines the heat flux and temperature variation throughout the entire trajectory, determines the appropriate TPS with dimensions returned to the main model, and returns the mass to the mass model.

In the above modules, subiterative loops are formed between the aerodynamic heat/heat transfer modules, which form a loop around the closure of the takeoff mass. The MDO task can be constructed by establishing the

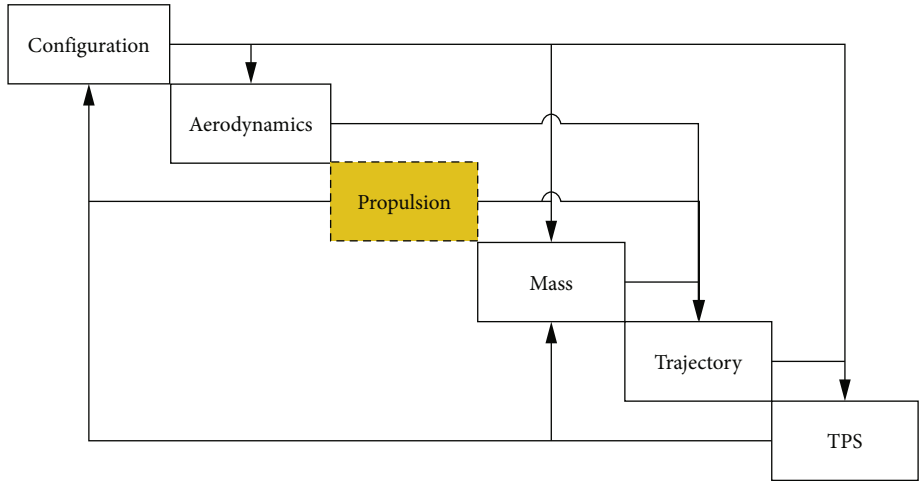

Figure 2: Multidisciplinary design structure matrix.

optimization objective function, design variables, and constraints in the outer layers.

3. Disciplinary Modeling of HGVs

3.1. Parameterized Geometric Model. The task of the parameterized geometric model is to parametrically model the configuration of the powered HGV to accurately describe the geometric characteristics of the powered HGV [28, 29].

In this paper, an MDO study is carried out based on the gliding body generated by the CST function. Equation (1) is used to define the windward and leeward sides of the gliding body, and Equation (2) is used to generate the blunt edges of the gliding body. The meanings of the parameters and the corresponding gliding bodies are shown in Figure 3.

$$\begin{cases} z_1 = H_1 \times \left(1 + \dfrac{y}{W/2}\right)^{N_{c1}} \times \left(1 - \dfrac{y}{W/2}\right)^{N_{c1}} \\ z_2 = H_2 \times \left(1 + \dfrac{y}{W/2}\right)^{N_{c2}} \times \left(1 - \dfrac{y}{W/2}\right)^{N_{c2}} - 2R \\ H_1 = x \tan\theta_1 \\ H_2 = x \tan\theta_2 \\ W_i = \dfrac{W_{\max}}{L_{\max}^{\,n}} x^n \end{cases} \tag{1}$$

$$\begin{cases} z_{\text{fillet\_up}} = R \times \left(1 - \dfrac{y_{\text{fillet}} - y_{\text{body}}}{R}\right)^{0.5} \times \left(1 + \dfrac{y_{\text{fillet}} - y_{\text{body}}}{R}\right)^{0.5} - R \\ z_{\text{fillet\_low}} = -R \times \left(1 - \dfrac{y_{\text{fillet}} - y_{\text{body}}}{R}\right)^{0.5} \times \left(1 + \dfrac{y_{\text{fillet}} - y_{\text{body}}}{R}\right)^{0.5} - R \end{cases} \tag{2}$$

The subscripts 1 and 2 correspond to the leeward and windward sides of the glider, respectively, and z_1 and z_2 are the points on the leeward and windward profiles, respectively. H_1 and H_2 are the maximum heights of the profile. N_{c1} and N_{c2} are the pattern line control parameters. θ_1 and θ_2 are the half-cone angles. n is the contour curve control parameter. $L_{\max}$ is the length of the vehicle; in this paper, the value of 5 m is taken. $W_{\max}$ is the maximum width of the bottom of the glider. W_i is the maximum section width of any section along the axial direction. R is the passivation radius. $z_{\text{fillet\_up}}$ and $z_{\text{fillet\_low}}$ are the z-coordinates of the blunt edges on the leeward and windward sides, respectively. y_{fillet} is the y-coordinate of the obtuse edge. y_{body} is the y-coordinate of the fuselage. Stretching a plurality of cross-sections of the upper surface profile and the lower surface profile, as well as the edges along the axial direction, generates a gliding body with smooth surface properties.

3.2. Computational Model for Hypersonic Aerodynamics. The task of the aerodynamic analysis model is to calculate the aerodynamic force data based on the selected flight envelope and configuration parameters. To ensure the accuracy of the aerodynamic results, high-precision aerodynamic calculation software [30, 31] is employed in this study. The CFD format used in this paper is as follows: the three-dimensional compressible Navier–Stokes equations are used as the governing equations, which are discretized using the finite volume method. In the computational solution process, the convective terms are discretized using the AUSMPW+ scheme, the viscous flux is discretized using a central difference scheme, and the time discretization is performed using the LU-SGS implicit scheme. The inflow boundary condition is set as the freestream condition, the outflow boundary condition is obtained through extrapolation from the centroid, the vehicle surface is treated with a nonslip isothermal wall condition, and the wall temperature is set at 300 K.

For the flight conditions $Ma = 10$, $H = 50$ km, and AOA $= -10 \sim 30°$, the local Reynolds number of the flight conditions is smaller than the transition Reynolds number, so the laminar flow model is chosen for the calculation. The computational format and grid used for numerical simulation have been verified in the literature [30, 31].

$$\text{Re}_{\text{tr}} = 6400 \times (Ma)^{3.66} \tag{3}$$

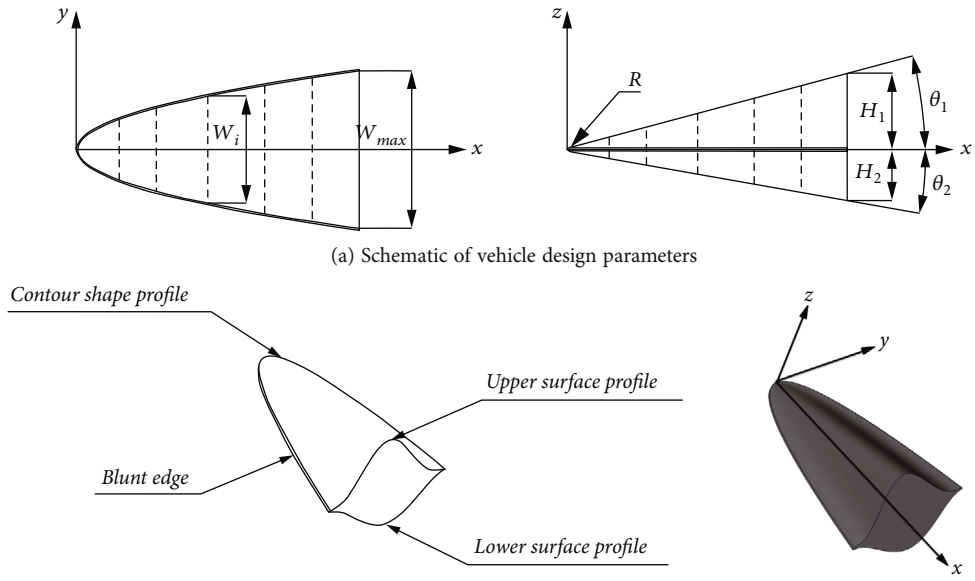

(a) Schematic of vehicle design parameters

(b) Schematic diagram of vehicle body shape lines and contour curves

(c) Generated vehicle configurations

Figure 3: Parameterized configuration of the vehicle.

3.3. Propulsion. The propulsion disciplinary analysis model consists of a geometric characteristic model, mass characteristic model, and performance analysis model. In this paper, the engine's geometric and mass characteristic models are classified under the geometric and mass disciplines, respectively, ensuring that the engine's assembly requirements are met by considering the volume ratio and volume. The performance analysis model is emphasized in the propulsion discipline. In the solid rocket engine performance analysis model, the thrust coefficient C_F is obtained by Equation (4).

$$C_F = \Gamma\sqrt{\frac{2k}{k-1}\left[1-\left(\frac{p_e}{p_c}\right)^{k-1/k}\right]} + \varepsilon\left(\frac{p_e}{p_c}-\frac{p_a}{p_c}\right) \quad (4)$$

The thrust P_T can be expressed as

$$P_T = C_F A_t P_c \quad (5)$$

The engine-specific impulse I_s can be expressed as

$$I_s = c^* C_F \quad (6)$$

where A_t is the area of the nozzle throat, P_c is the combustion chamber pressure, P_e is the nozzle outlet pressure, P_a is the atmospheric ambient pressure, k is the gas-specific heat ratio, c^* is the characteristic propellant velocity, and ε is the nozzle expansion ratio.

The mass of the engine used in this paper is 200 kg (of which the mass of solid fuel is 100 kg), the magnitude of thrust is 3000 N, and the specific impulse is 3000 (N·s/kg) [12]. Taking the fuel density as 1.7 g/cm^3, the fuel volume is 58.9 dm^3. Referring to the work of Miao et al. [32] and Wu et al. [33], the dimensions of the engine are initially given as 100 mm in length and 32 mm in diameter. The engine volume is 80.4 dm^3. For the vehicle to meet the engine mounting requirements, the following two points are of primary consideration. The first point is that the vehicle should have a volume of 80.4 dm^3 reserved for the engine, in addition to the space occupied by other loads such as flight controls and batteries. In practice, the internal volume of the vehicle should not be less than 1 m^3 to ensure that there is sufficient space to install the vehicle subsystems. The second point is that solid rocket engines are generally mounted on the bottom of the vehicle, which also places certain requirements on the dimensions of the bottom cross-section of the vehicle. Therefore, calculations are made to give lower limits for the design variables affecting the dimensions of the bottom cross-section, as shown in Table 1 (including the upper half-cone angle θ_1, the lower half-cone angle θ_2, and the maximum width of the bottom $W_{\max}$).

3.4. Model for Analysis of Mass Properties. The mass estimate method proposed by Fan, Xu, and Hao [34] is adopted. The total mass of the vehicle is divided into propulsion system mass, structural mass, subsystem mass, payload mass, and TPS mass.

The reentry mass of the vehicle can be calculated as

$$m_0 = m_s + m_{pl} + m_{im} + m_f + m_t \quad (7)$$

where m_0 is the initial mass of the vehicle; m_s and m_{im} are the mass of the body structure and subsystem, respectively; m_{pl} is the mass of the payload; m_f is the mass of the solid rocket engine; and m_t is the mass of the TPS.

m_s is determined primarily by the surface area of the vehicle. m_{im} and m_{pl} are given by the tactical and technical requirements. m_f has been identified in subsection 3.3.

Table 1: Configuration optimization results for powered HGV.

Parameters	Before optimization	After optimization	Value range
$\theta_1/(^\circ)$	5	4.51	[3, 7]
$\theta_2/(^\circ)$	3.5	3.33	[2, 5]
$W_{\max}/(\mathrm{m})$	2.4	1.9	[1.8, 3]
N_{c1}	1.5	2.1	[1.5, 5]
N_{c2}	5	2.22	[1.5, 5]
n	0.6	0.51	[0.4, 0.6]
$R/(\mathrm{mm})$	12.5	5.0	[5, 20]

Based on experience, m_t is estimated to be 13% of the total mass of the vehicle. The determination of the final m_t can be found in subsection 5.2.

3.5. Trajectory. Trajectory analysis is an essential means of establishing the relationship between tactical technical indicators and overall parameters, as well as the basis for testing whether the vehicle can fulfill its intended mission. The task of trajectory analysis is to calculate and determine the flight characteristics of the powered HGV according to the results of aerodynamics, propulsion, mass, and other disciplines and to provide relevant data support for the analysis of the thermal protection discipline. Therefore, the accuracy of the trajectory analysis model is crucial. In this paper, the controlled mass dynamics model is used to describe the flight characteristics of the powered HGV, and its mathematical model is established as

$$\begin{cases} \dfrac{\mathrm{d}v}{\mathrm{d}t} = \dfrac{P_T \cos\alpha - F_D}{m} - g\sin\gamma \\ \dfrac{\mathrm{d}\gamma}{\mathrm{d}t} = \dfrac{P_T \sin\alpha - F_L}{mv} - \left(\dfrac{v}{R_0 + h} - \dfrac{g}{v}\right)\cos\gamma \\ \dfrac{\mathrm{d}L}{\mathrm{d}t} = \dfrac{R_0}{R_0 + h} v\cos\gamma \\ \dfrac{\mathrm{d}h}{\mathrm{d}t} = v\sin\gamma \\ \dfrac{\mathrm{d}m}{\mathrm{d}t} = -\dot{m}_{\mathrm{cc}} \end{cases} \tag{8}$$

where v is the velocity, γ is the flight path angle, h is the altitude, L is the range, m is the mass, P_T is the engine thrust, F_D is the drag, F_L is the lift, g is the gravitational acceleration, R_0 is the mean radius of the earth, and m_{cc} is the fuel flow rate.

Generally, the reentry vehicle trajectory optimization can be assumed to be an optimal control problem that maximizes/minimizes the optimization objective while satisfying the initial and final flight state conditions and the requirements for heat flux, overloading, and dynamic pressure during the gliding process. The commonly used methods for solving such problems are direct methods [35] and indirect methods [36]. In this paper, the hp-Radau pseudospectral method, widely used in direct ways, is applied to solve the established trajectory optimization problem.

It is worth noting that the trajectory optimization for a powered HGV is different from that of an unpowered HGV, as the former needs to consider the control effect of step thrust, and the trajectory optimization process must address the bang-bang control. The hp-Radau pseudospectral method can effectively solve the step control problem while preserving the global trajectory optimization properties by discretizing the trajectory into segments and setting continuity conditions between them [35].

3.6. Computational Model of the Aerodynamic Heat/TPS Design. The transient heat flux density on the vehicle surface is determined using widely used empirical formulas in engineering. Different empirical formulas are selected for different regions of the vehicle surface based on the varying degree of heating in each area [37].

3.6.1. Leading Edge Stagnation Point. Kemp and Riddell's stagnation point aerodynamic heating rate calculation model as follows:

$$q_{ws} = \frac{131884.2}{\sqrt{R_N}} \left(\frac{\rho_\infty}{\rho_0}\right)^{0.5} \left(\frac{v_\infty}{v_c}\right)^{3.25} \left(1 - \frac{h_w}{h_s}\right) \tag{9}$$

where q_{ws} is the stagnation point aerodynamic heating rate, v_∞ is the incoming flow velocity, ρ_∞ is the incoming flow density, R_N is the stagnation point curvature circle radius, $\rho_0 1225\mathrm{kg/m}^3$, $v_c 7900\mathrm{m/s}$, h_w is the wall enthalpy, and h_s is the stagnation enthalpy.

3.6.2. Fuselage and Other Areas. Using the Eckert reference enthalpy method, the reference enthalpy h^* is determined by the combination of the wall and outflow conditions and can be expressed as

$$h^* = 0.19h_r + 0.23h_e + 0.58h_w \tag{10}$$

where h_r is the enthalpy of recovery, subscript "e" denotes the boundary layer outer edge parameter, and superscript "$*$" indicates the reference value.

The heat flux density is calculated using the flat plate heat flux formula, which is derived from the Blasius surface friction formula and its relationship with the Reynolds number. Calculating the Stanton number St^* can be obtained from the Reynolds number relationship of the flat plate.

$$St^* = \frac{C_f{}^*}{2}\mathrm{Pr}^* - \frac{2}{3} \tag{11}$$

In Equation (11), $C_f{}^*$ is calculated using the Blasius formula for incompressible flow.

$$C_f{}^* = \frac{0.664}{\sqrt{\mathrm{Re}^*}} \tag{12}$$

The heat flux density equation for a flat plate laminar flow is given by

$$q = St^* C_p^* \rho^* v_e (h_r - h_w) \tag{13}$$

In Equations (11), (12), and (13), Re*, $C_p{}^*$, Pr*, and ρ^* are the Reynolds number, specific heat capacity, Prandtl number, and gas density at the reference enthalpy h^*, respectively, and v_e is the gas flow velocity at the boundary layer's outer edge.

When sizing a TPS for a vehicle, the temperature of the vehicle's surface needs to be known. A conservative value is obtained using the equilibrium temperature of radiant heat at the wall surface. Based on the following assumptions: the heat flow into the interior of the material is 0, and the convective heat transfer is balanced with the radiant heat flow at the surface of the material, it can be concluded that the wall radiant equilibrium temperature is calculated as

$$q_{gw}\left(1 - \frac{h_w}{h_r}\right) - \varepsilon\sigma {T_w}^4 = 0 \tag{14}$$

where q_{gw} is the gas heat flow at the wall, σ is the Stefan–Boltzmann constant with a magnitude of $5.670367 \times 10\text{e} - 8\ \text{W}/(\text{m}^2\text{k}^4)$, ε is the radiation coefficient of the vehicle surface (usually 0.7~0.9), and T_w is the temperature of the vehicle wall.

For heat transfer/TPS modeling, the model is used to predict internal heat transfer characteristics and determine the needed TPS dimensions over a range of service temperatures. It is inextricably linked to the pneumatic heat module, where the heat transfer analysis takes the external heat flow as input. The external heat flow transient calculations require the wall transient temperatures to be given based on the current heat transfer analysis, and the two form a tight iterative loop that interleaves the calculations at the time step. In the heat transfer analysis, it is assumed that the heat shield material is isotropic. Only one-dimensional heat flow and temperature calculations along the thickness direction are considered. The complete mathematical description includes the differential equations for thermal conductivity and the corresponding boundary conditions.

The differential equation for heat transfer is obtained from the conservation of energy.

$$\rho c \frac{\partial}{\partial t}(T) = \frac{\partial}{\partial x}\left(\lambda \frac{\partial T}{\partial x}\right) \tag{15}$$

In Equation (15), ρ, c, and λ are the density, specific heat capacity, and thermal conductivity of the material, respectively, and they are functions of temperature.

The adiabatic wall boundary condition is used on the inner boundary surface, and the heat flow density boundary condition is used on the outer boundary surface with the following expression.

$$q_w = q_w(t) = q_{\text{cond}} + \varepsilon\sigma T_w^4 \tag{16}$$

where q_w is the heat flux at the wall and q_{cond} is the heat conduction loss.

Discretization of Equation (16) yields

$$\begin{aligned} &\frac{1}{R_{i-1}^{t+\Delta t}} T_{i-1}^{t+\Delta t} - \left[\frac{1}{R_i^{t+\Delta t}} + \frac{1}{R_{i-1}^{t+\Delta t}} + (\rho c)_i^{t+\Delta t}\frac{\Delta x_i}{\Delta t}\right] T_i^{t+\Delta t} \\ &\quad + \frac{1}{R_i^{t+\Delta t}} T_{i+1}^{t+\Delta t} = -(\rho c)_i^t \frac{\Delta x_i}{\Delta t} T_i^t \end{aligned} \tag{17}$$

In Formula (17),

$$R_{\text{e}}^{t+\Delta t} = \frac{\delta x_{\text{e}}}{\lambda_{\text{e}}^{t+\Delta t}} = \frac{\delta x_{e-}}{\lambda_i^{t+\Delta t}} + \frac{\delta x_{\text{e}+}}{\lambda_{i+1}^{t+\Delta t}} = \frac{\delta x_i}{2\lambda_i^{t+\Delta t}} + \frac{\delta x_i}{2\lambda_{i+1}^{t+\Delta t}} \tag{18}$$

Discretization of Equation (18) yields

$$\begin{aligned} &\left[(\rho c)_1^{t+\Delta t}\frac{\Delta x_1}{\Delta t} + \frac{1}{R_1^{t+\Delta t}}\right] T_1^{t+\Delta t} - \frac{1}{R_1^{t+\Delta t}} T_2^{t+\Delta t} \\ &\quad = -\varepsilon\sigma \cdot \left(T_1^{t+\Delta t}\right)^4 + q(t+\Delta t) + (\rho c)_1^t \frac{\Delta x_1}{\Delta t} T_1^t \end{aligned} \tag{19}$$

Due to the different material properties of the structural layer and the heat protection layer, the above model needs to be solved in layers to calculate the temperature and heat flux history.

4. Multidisciplinary Optimization Problem Definition

To establish a nonlinear programming (NLP) problem, one must determine the objective function, constraint conditions, and design variables. An MDO problem synthesizes individual disciplinary optimization problems rather than a simple superposition. It should include all possible constraints and design variables from each discipline while considering potential conflicts between disciplines to avoid "overconstraining" and "nonindependent design variables."

4.1. Objective Function. According to the mission characteristics of the powered HGV and the requirements of the tactical technical indicators, the maximum range L under the given mission conditions is selected as the objective function in this paper, as shown in Equation (20).

$$\max\ (J = L) \tag{20}$$

4.2. Design Variables. The overall design scheme of a hypersonic glide vehicle involves optimizing variables in four disciplines: geometry, trajectory, mass, and thermal protection. However, in the case of the heat transfer/TPS discipline, the TPS thickness is determined iteratively, while the output of the mass discipline is dependent on the results obtained from other disciplines. As a result, these variables are not included in the system-level optimization. The final selection

includes variables that significantly impact the overall performance, such as

1. Configuration variables: the following 7 design variables are included: upper half-taper angle θ_1, lower half-taper angle θ_2, maximum width at the bottom W_{max}, upper surface profile parameter N_{c1}, lower surface profile parameter N_{c2}, contour curve control parameter n, and passivation radius R.
2. Trajectory variables: include the glide reentry parameters of altitude h, velocity v, flight path angle γ, angle of attack α, and thrust P_T. These variables impact reentry overloads, dynamic pressure, and aerodynamic heating characteristics.

4.3. Constraints. The main constraints of the overall design are as follows.

1. Configuration

a. Maximum profile size limitations.

b. Internal volume $V_{in} > 1\,m^3$ (to accommodate equipment installation, including solid engine).

2. Propulsion

a. Engine structural mass constraint.

3. Trajectory

a. Reentry starting velocity $v = 6000$ m/s.

b. Reentry starting altitude $h = 80$ km.

c. Reentry finally velocity $v > 2000$ m/s.

d. Reentry finally altitude $h > 30$ km.

e. Reentry maximum dynamic pressure $q < 120$ kPa.

f. Reentry maximum overload $n < 5$ g.

g. Reentry maximum heat flux rate $\dot{Q} \leq 1200\,W/m^2$.

4. TPS

a. Maximum cabin temperature $T < 150^{\circ}$.

b. Heat-proof structural mass constraints.

5. System Integration and Optimization

5.1. Sampling Design and Surrogate Modeling. To reduce the computational complexity of MDO problems and save solution time, the kriging algorithm is used to construct a surrogate model to replace the computationally expensive accurate model.

Kriging surrogate models are a type of interpolation technique based on mathematical statistics. Their objective is to simulate the information of unknown points by utilizing the data from a subset of known points. Due to their strong capability to approximate nonlinear systems, kriging models have been extensively researched and applied in various fields, such as aerospace, agriculture, and mechanical dynamics [38, 39]. Unlike conventional black-box models, kriging models do not require establishing a specific parameterized mathematical model. Moreover, compared to other surrogate models, one notable feature of kriging models is that they provide estimated values for unknown functions and enable error analysis and estimation of these predictions. As a result, they prove to be highly effective and practical for range prediction scenarios involving multiple influencing factors.

The foundation of constructing a kriging surrogate model lies in sample information. Uniformly distributed samples can provide information across the entire design space, allowing the constructed model to capture the trend and variation of the true objective function. On the other hand, uneven sample information can lead to low simulation accuracy of the kriging surrogate model and even result in erroneous approximation models. Latin hypercube sampling (LHS) is employed in this study as the sampling method for the kriging surrogate model. LHS ensures uniform sampling without clustering and guarantees the comprehensiveness of the samples [40].

5.2. System Integration and Optimization Process. The integration of MDO problems requires the selection of specific optimization computational architectures to organize the optimization problems, such as MDF, CO, and CSSO. According to the design structure matrix shown in Figure 2, the interdisciplinary iterative loop is mass-balanced, which belongs to a typical coupling-intensive problem, so this paper chooses the multidisciplinary feasible method.

According to the MDO problem defined in the previous section, the computational modules of each discipline are integrated into the software framework Isight, and the task flow and data mapping relationship of disciplines are established. The kriging agent model of MDO is constructed to improve the computational efficiency; the optimal Latin hypercubic sampling method is selected to take 100 points when sampling, and the optimization algorithm selection of the agent model is also essential. The nongradient algorithm does not depend on the choice of initial value points and has global convergence characteristics. Nevertheless, the optimization process requires many iterations, and the computational efficiency is very low. In contrast, the gradient algorithm is susceptible to the initial value and derivative information and easily falls into the local optimum. Nevertheless, it requires fewer iterations, and the convergence speed is faster. Considering the sizeable computational scale of the powered HGV, the gradient algorithm is selected to solve the problem with higher efficiency.

The process of the MDO for the powered HGV is shown in Figure 4.

The detailed process of the design optimization is described below.

1. Determine the initial layout of the vehicle according to the mission plan and overall requirements.

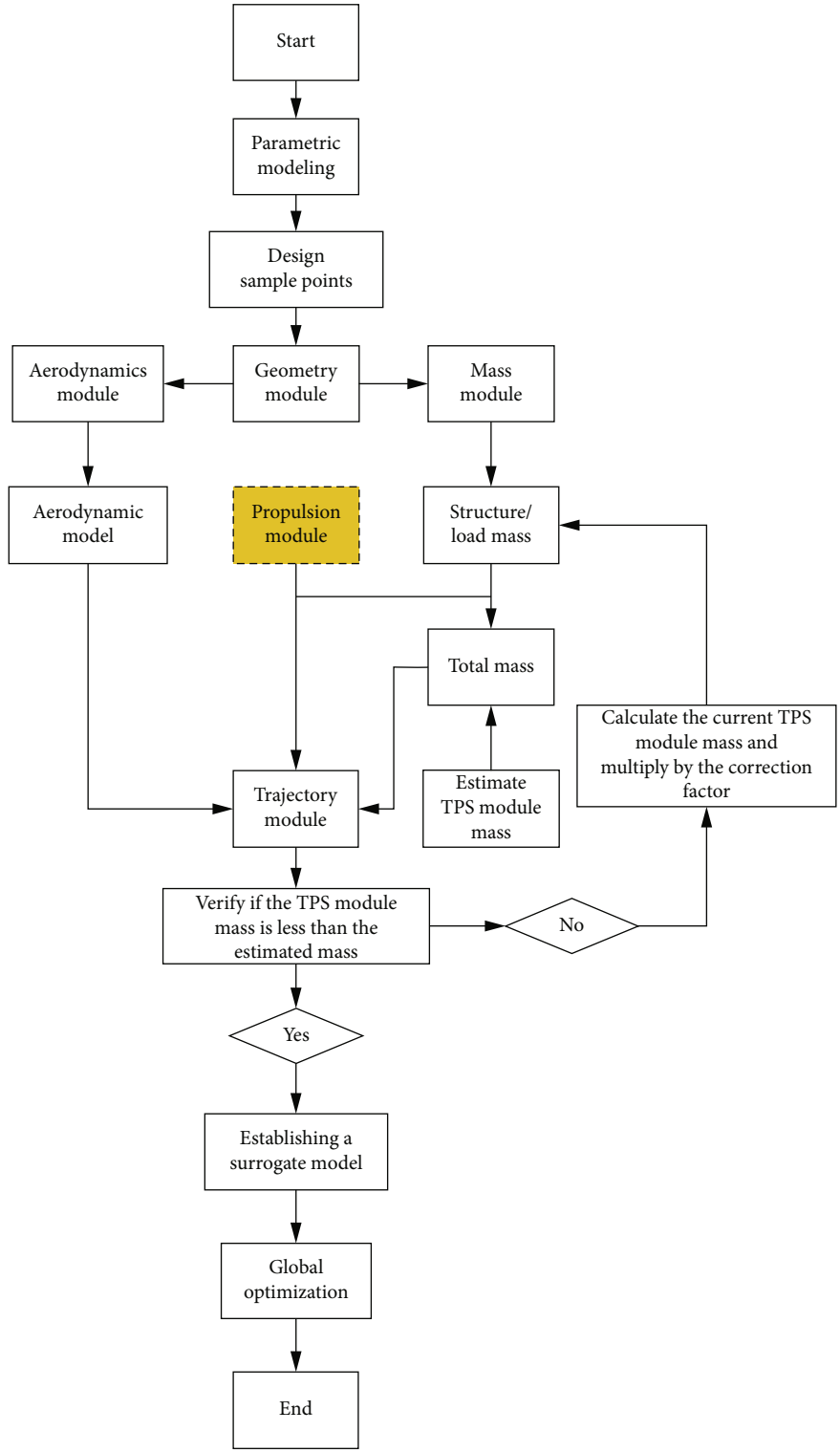

Figure 4: Process of multidisciplinary design optimization.

2. Determine the geometry design variables according to the research objectives and select the appropriate method to generate the sample points of the design variables.

3. According to the selected sample points of the geometry design variables, the parametric modeling method is used to generate the corresponding configuration of the vehicle.

4. Transfer the configuration files to the mass and aerodynamic disciplines. For the mass discipline, estimate the structural mass of the whole vehicle based on the structural characteristics and estimate the mass of the TPS (approximately 13% of the total weight of the entire vehicle), together with the loads of the whole vehicle and the mass of the engine, to estimate the mass of the real vehicle. The CFD program is called to solve the aerodynamic model for the aerodynamic discipline.
5. Optimization will be performed on the reentry trajectory of the vehicle based on the overall scheme requirements and in conjunction with the vehicle mass, aerodynamic model, and propulsion model provided in Step 4.
6. According to the reentry trajectory obtained in Step 5, calculate the exact mass of the TPS. If it exceeds the estimated mass, increase the mass of the TPS and recalculate the trajectory.
7. Evaluate the set performance, analyze the performance indicators of all sample points, and select an appropriate surrogate model to establish a global surrogate model.
8. Select the appropriate optimization algorithm and perform global optimization to complete the MDO process.

6. MDO Results for the Powered HGV

The multidisciplinary optimization task was performed on a computational server containing 800 CPUs (40 cores per computing node, with 20 computing nodes), taking approximately 200 h. The primary computational workload was attributed to the aerodynamics analysis based on the NS equations. A functional relationship between the lift and drag coefficients and the angle of attack for each sample point was provided. The angle of attack states to be calculated were set at −10°, −5°, 0°, 3°, 5°, 10°, 15°, 20°, 25°, and 30°. In parallel execution mode, it took 3–4 h to compute one state using every two nodes.

The accuracy and degree of fitting of the surrogate model are measured by the coefficient of determination (R^2) and the maximum relative error (MRE) [41]; in this section, the surrogate model has high accuracy with a coefficient of determination of 0.998 and an MRE of 0.031.

6.1. Optimization Results for Geometry and Aerodynamic Disciplines. Table 1 and Figure 5 present the powered HGV configuration optimization results.

The comparison between configurations of the hypersonic vehicle before and after optimization is demonstrated in Figure 5. The optimized powered HGV has undergone several changes, resulting in reductions of 9.8% and 4.8% in θ_1 and θ_2, respectively, and a reduction of 20.8% in W_{max}, compared to the original powered HGV. The width of the vehicle body has been significantly reduced, leading to a 15% decrease in the vehicle's weight, which is beneficial for increasing its range. Additionally, N_{c1} is increased by 40%, N_{c2} is decreased by 55.6%, n is reduced by 15%, and R is decreased by 58.3%. These changes have all contributed to an increase in the lift-to-drag ratio of the vehicle, thereby enhancing its maneuverability and range.

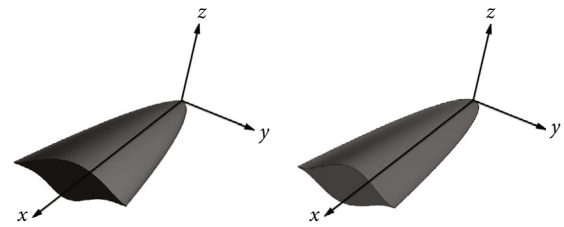

(a) Configuration before optimization (b) Configuration after optimization

Figure 5: Comparison between configurations of the powered HGV before and after optimization.

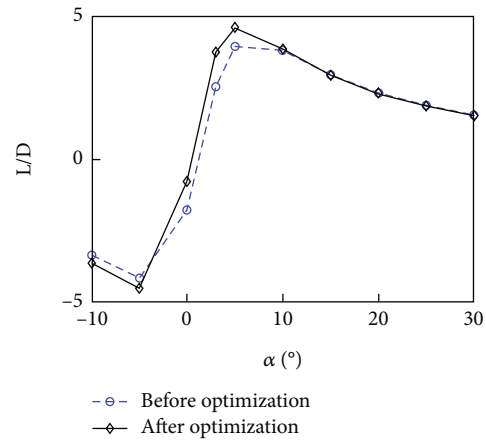

Figure 6: Variation in the lift-to-drag ratio with the angle of attack for the powered HGV before and after optimization.

Figure 6 shows the variation curve of the lift-to-drag ratio of the powered HGV to the angle of attack. It shows that the variation rule of the lift-to-drag ratio with the angle of attack remains the same before and after the optimization of the vehicle. At negative angles of attack, the lift-to-drag ratio decreases first and then increases with increasing angle of attack. At positive angles of attack, the lift-to-drag ratio rises first and then decreases with increasing angle of attack. The maximum lift-to-drag ratio occurs at an approximately 5° angle of attack. During the reentry process of the vehicle, the angle of attack mainly stays within the range of 0° to 10°. Within this range, the lift-to-drag ratio of the optimized powered HGV is significantly higher than that of the preoptimized powered HGV, thus benefiting the improvement of the powered HGV range.

6.2. Optimization Results of the Trajectory. Figure 7 compares the trajectory of the HGV before and after optimization. Figures 7(a)–7(d) show the variation in the HGV's state variables with time, and both trajectories accurately

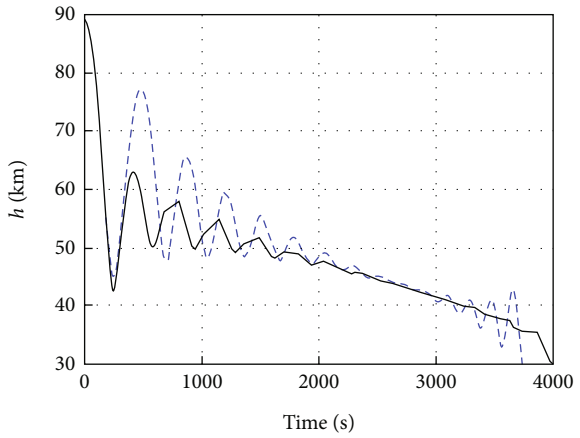

(a) Altitude history over time

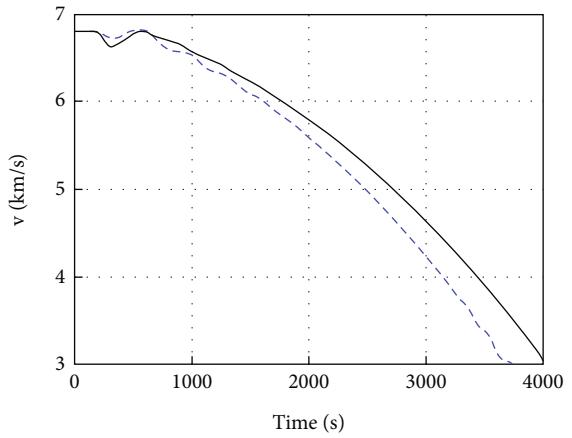

(b) Velocity history over time

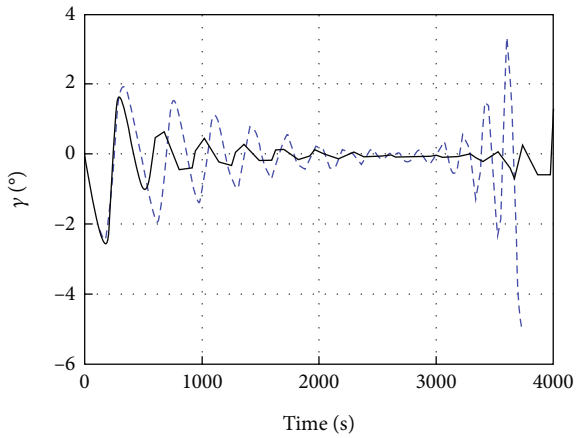

(c) Flight path angle over time

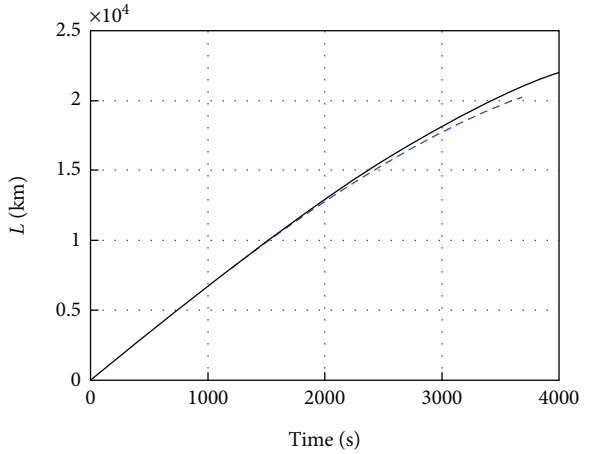

(d) Range history over time

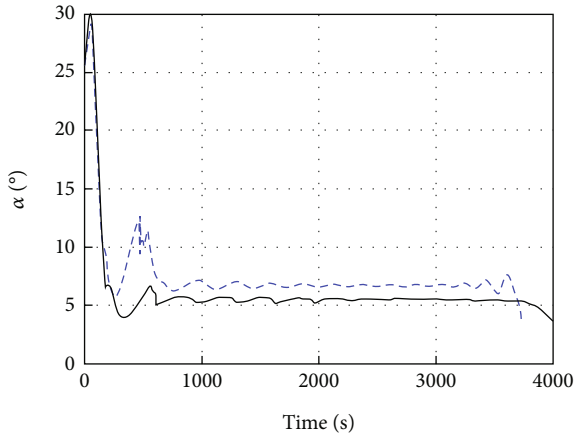

(e) Angle of attack history over time

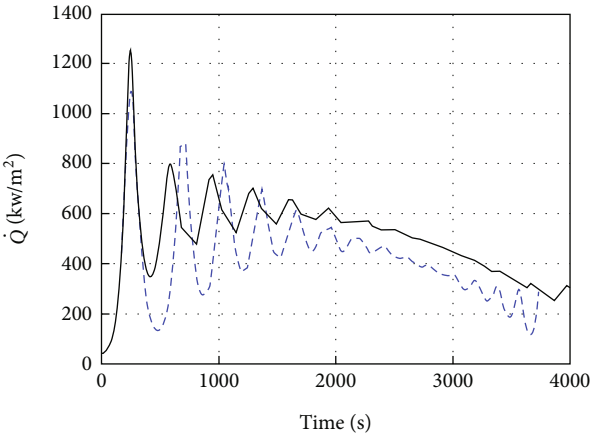

(f) Heat flow history over time

Figure 7: Continued.

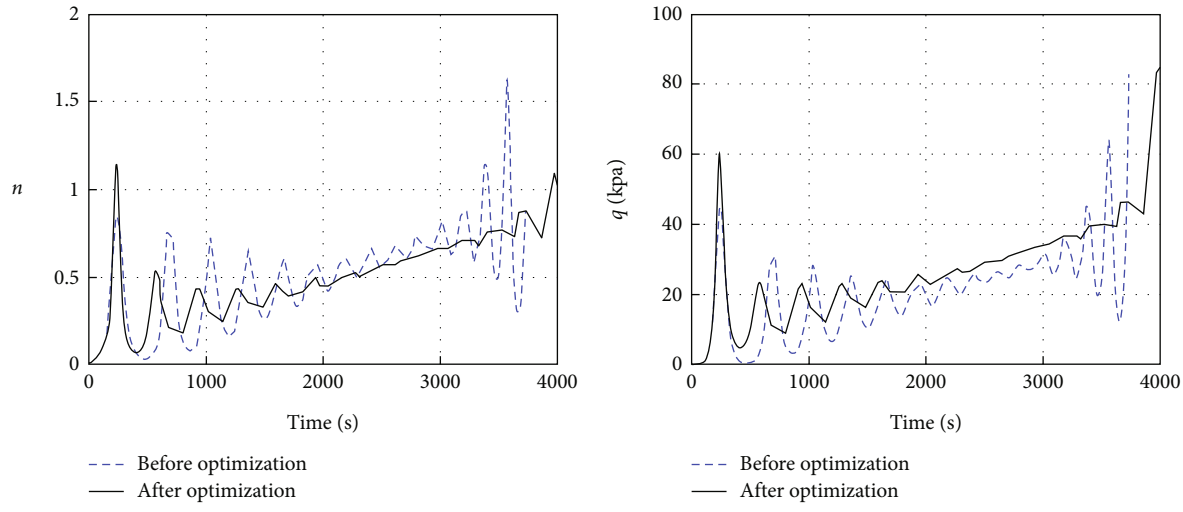

(g) Overload history over time

(h) Dynamic pressure history with time

Figure 7: The course of the state quantities with time during the reentry of the HGV.

satisfy the initial and final boundary conditions. Figures 7(a) and 7(c) show that the height variation is smoother after optimization, and the HGV trajectory is more stable. Figure 7(b) shows that the velocity decay is slower after optimization, resulting in a longer flight time and thus increasing the total range. After optimization, the whole range of the HGV reaches up to 22,070 km, which is 1694 km larger than that before optimization, or approximately 8.37% more.

Figure 7(e) shows the variation history of the angle of attack with time before and after optimization, and the variation in the angle of attack is relatively smooth, which indicates that the vehicle will not make unrealistic sudden movements. The change histories of heat flow, overload, and dynamic pressure with time are shown in Figures 7(f) and 7(g). The vehicle trajectories before and after optimization satisfy the path constraints. The path constraint values of the optimized vehicle trajectory are smaller than those of the preoptimized vehicle trajectory in most of the gliding time. At the beginning of the reentry process, the main task of the vehicle is to avoid reaching the heat flux boundaries. Subsequently, the main task is to control the overload and dynamic pressure values within a reasonable interval.

7. Comparison of Optimization Results for Coupled/Decoupled Propulsion Discipline

Research has been conducted in [12–17] on the trajectory optimization problem of powered HGVs. This can be understood as initially performing an MDO for the vehicle under unpowered conditions, with the coupling between disciplines illustrated in Figure 2. The MDO process is depicted in Figure 4 (excluding the propulsion discipline marked in yellow within both Figures 2 and 4). Subsequently, the optimized vehicle configuration is used for trajectory optimization with power replenishment. The specific design process is depicted in Figure 8. During the overall MDO to obtain the optimal shape of such vehicles, the influence of the propulsion discipline was not taken into account, thus assuming a decoupling of the propulsion discipline. In the trajectory optimization process with power replenishment, the design variables are solely related to the trajectory discipline due to the fixed vehicle configuration. Consequently, the potential of powered HGVs cannot be fully realized. To demonstrate the importance of coupling the propulsion discipline in the overall optimization design process of the powered

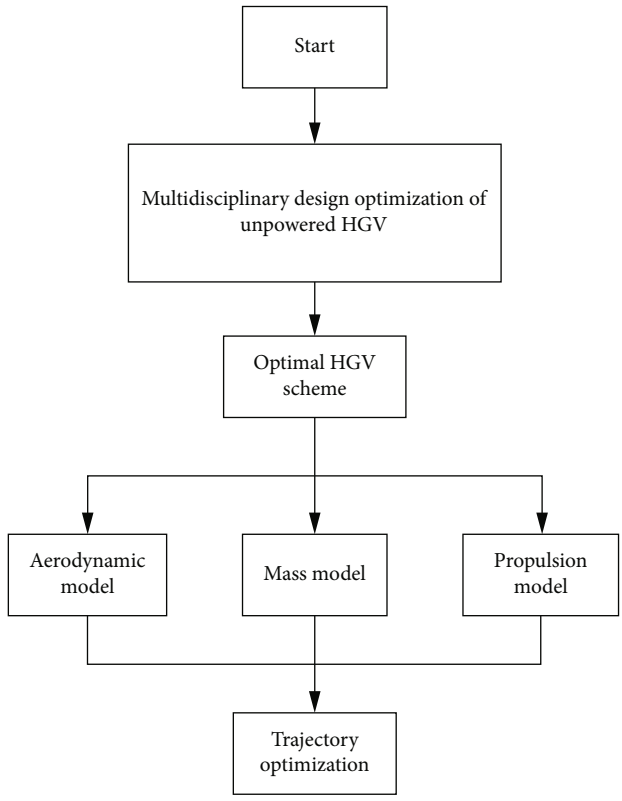

Figure 8: Trajectory optimization process of the powered HGV in existing research.

Table 2: Configuration optimization results for powered HGV (decoupled propulsion/coupled propulsion).

Parameters	Decoupled propulsion	Coupled propulsion	Value range
θ_1/(°)	5.4	4.51	[3, 7]
θ_2/(°)	2	3.33	[2, 5]
W_{max}/(m)	1.8	1.9	[1.8, 3]
N_{c1}	1.5	2.1	[1.5, 5]
N_{c2}	4	2.22	[1.5, 5]
n	0.6	0.51	[0.4, 0.6]
R/(mm)	5	5.0	[5, 20]

HGV, the design process shown in Figure 8 was adopted to optimize the baseline vehicle configuration in this paper. The optimized vehicle configuration without coupling the propulsion discipline and its trajectory with power was obtained. Subsequently, the results of this section were compared with those of Section 6.

In this section, the surrogate model has high accuracy with a coefficient of determination of 0.997 and an MRE of 0.034.

7.1. Optimization Results for Geometry and Aerodynamic Disciplines. The results of the configuration of the powered HGV optimized by the coupled/decoupled propulsion disciplines are given in Table 2 and Figure 9.

A comparison of the optimized vehicle configuration by the coupled/decoupled propulsion disciplines is shown in Figure 9. Compared with the vehicle optimized by decoupled propulsion disciplines, the upper half-cone angle θ_1 of the vehicle optimized by coupled propulsion disciplines is reduced by 16.48%, the lower half-cone angle θ_2 is increased by 66.5%, the maximum width of the bottom W_{max} is increased by 5.56%, the fuselage width of the vehicle is slightly raised, and the mass of the vehicle is unchanged. The upper surface profile parameter N_{c1} rises by 40%, the lower surface profile parameter N_{c2} decreases by 44.5%, and the contour index parameter n reduces by 15%, all of which are conducive to increasing the lift-to-drag ratio of the vehicle, thus enhancing the maneuverability and range of the vehicle. The passivation radius R is kept constant at the lower limit of the design variables, and the smaller the value of R is, the larger the vehicle lift-to-drag ratio.

As shown in Figure 10, the change rule of the lift-to-drag ratio of the vehicles obtained from the optimization of coupled/decoupled propulsion disciplines is the same; with the increase in the angle of attack, the lift-resistance ratio shows a trend of decreasing first, then increasing, and then declining after reaching the maximum lift-resistance ratio. Among them, the maximum lift-to-drag ratio appeared at an approximately 5° angle of attack. During the reentry process, the angle of attack of the vehicle is kept in the range of 0° to 10° during the primary working time, and the lift-to-drag ratio of the vehicle optimized by the coupled propulsion disciplines is larger than that of the vehicle optimized by the decoupled propulsion discipline in this angle of attack interval.

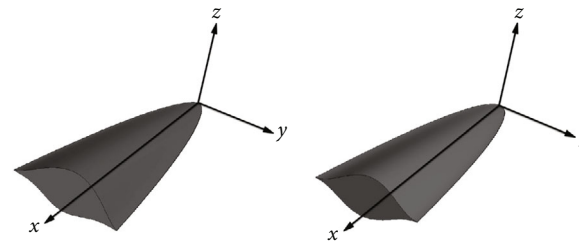

(a) Configuration for decoupled propulsion discipline (b) Configuration for coupled propulsion discipline

Figure 9: Comparison of the configurations optimized by the coupled/decoupled propulsion discipline.

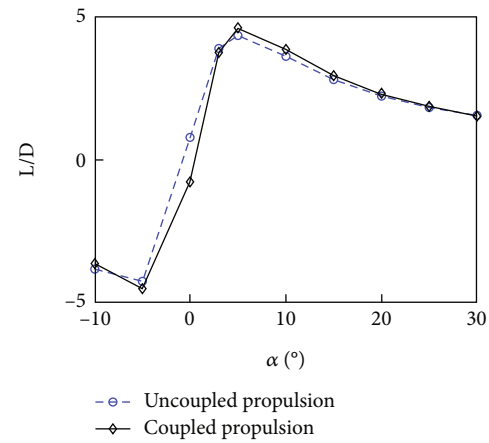

Figure 10: Variation in the lift-to-drag ratio with the angle of attack for the vehicle optimized by the coupled/decoupled propulsion discipline.

7.2. Optimization Results of the Trajectory. The trajectories of HGVs optimized by coupled/decoupled propulsion discipline are compared in Figure 11.

In Figures 11(a)–11(d), the vehicle state variable change process with time is shown, and both trajectories accurately satisfy the initial and final boundary conditions. The vehicle trajectory optimized by coupled propulsion disciplines is relatively smoother, and its velocity decays slower, thus increasing the flight time. The range of the optimized vehicle increases by 890 km, or approximately 3.87% more.

The angle of attack change curves are shown in Figure 11(e), and the angles of attack of both trajectories are within the constraints. The changes are relatively smooth, indicating that the vehicle will not make unrealistic sudden movements.

The heat flux, overload, and dynamic pressure change curves are shown in Figures 11(f)–11(h). Both trajectories satisfy the path constraints, and the trajectory path constraint values of the two trajectories are similar in most of the gliding time; at the end of the gliding section, the values of the overload and the dynamic pressure of the vehicle optimized by decoupled propulsion discipline show a large jitter. At the beginning of the reentry process, the main task of the vehicle is to avoid reaching the heat flux boundaries. Subsequently, the main task is to control the overload and dynamic pressure values within a reasonable interval.

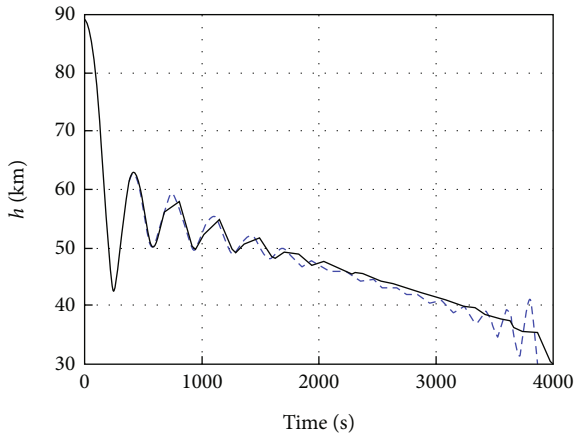

(a) Altitude history over time

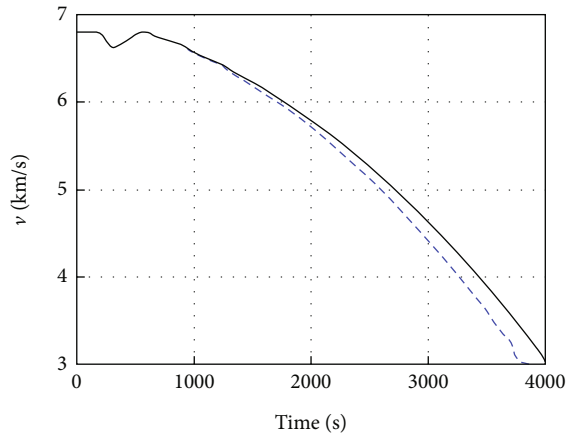

(b) Velocity history over time

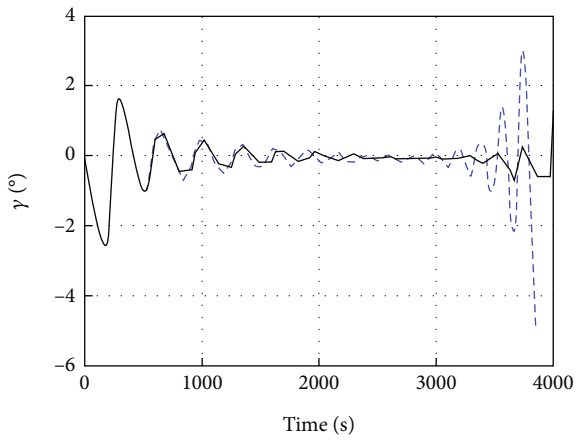

(c) Flight path angle over time

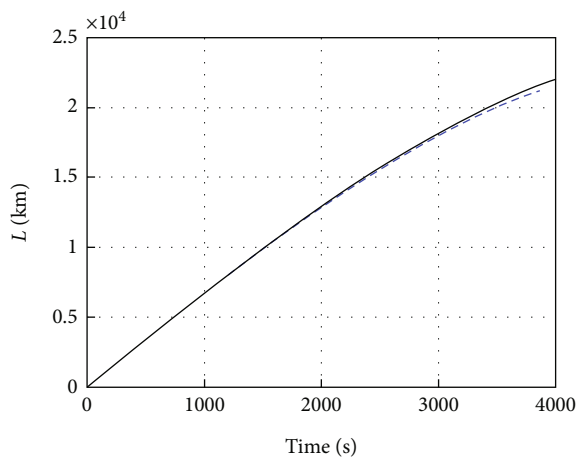

(d) Range history over time

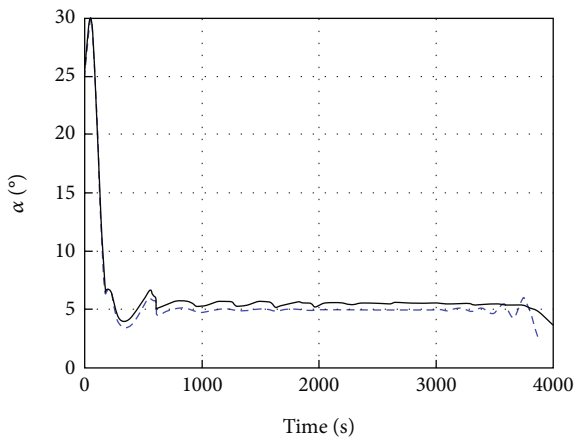

(e) Angle of attack history over time

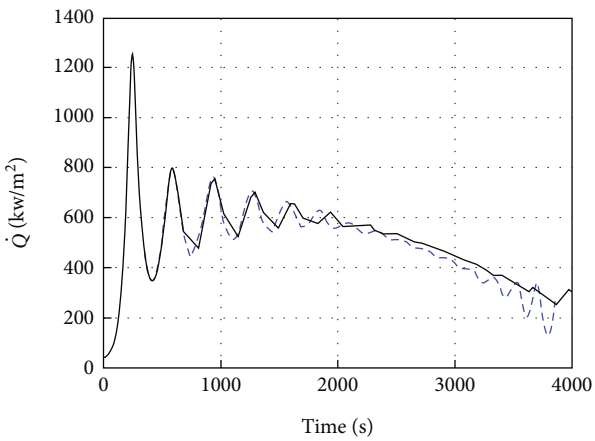

(f) Heat flux history over time

Figure 11: Continued.

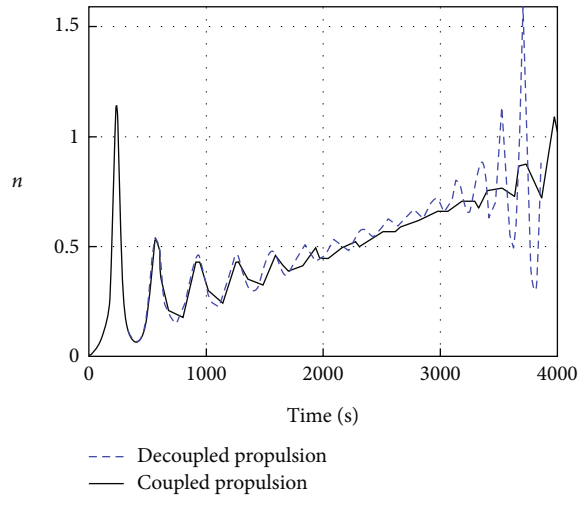

(g) Overload history over time

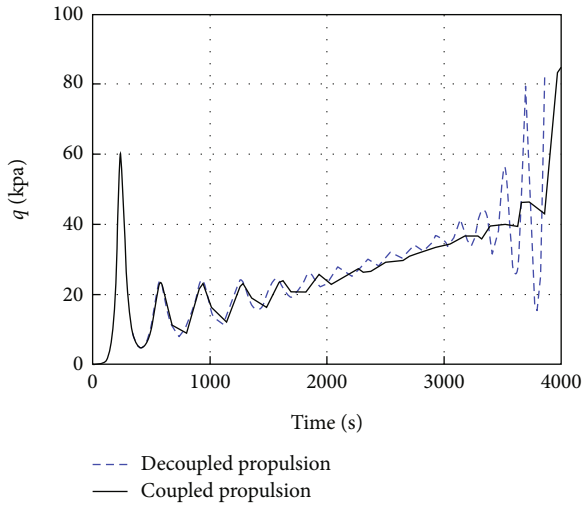

(h) Dynamic pressure history with time

Figure 11: The course of the state variables with time during the reentry of the HGV.

8. Conclusion

Aiming at the two problems in the research process of trajectory optimization of powered HGVs without fully considering the overall design constraints and interdisciplinary coupling, this paper studies the application of MDO in its overall design process. The systematic study of multidisciplinary optimal design task planning and demand analysis, multidisciplinary modeling, system definition and design, and system integration and solution significantly reduces the computational cost of high-fidelity CFD simulation through the introduction of the agent model method in the system integration and optimization stage and finally validates the multidisciplinary optimal design method through numerical examples and compares the optimization results of powered HGV designed by coupled/decoupled propulsion disciplines. The following conclusions are drawn.

1. According to the characteristics of the overall design of the powered HGV and the coupling between disciplines, a system integration optimization strategy based on the kriging agent model is proposed, which better solves the problems of the complexity of the MDO process, a large amount of computation, and time-consuming solving. It provides a better solution for obtaining the optimal solution of the system.
2. Under the premise of satisfying various design constraints, the HGV optimized by the MDO method established in this paper has improved its range index by 1694 km, or approximately 8.37% more compared to the optimization before, which verifies the reliability of the proposed method.
3. The optimized design of the powered HGV with decoupled propulsion disciplines is carried out and compared with the results of the coupled propulsion disciplines, and the range index of the vehicle optimized by the coupled propulsion disciplines is improved by 890 km, or approximately 3.87% more under the condition of meeting the mission requirements and overall constraints. This shows that for the powered HGV, it is necessary to comprehensively consider the improvement of the vehicle performance from the overall multidisciplinary optimization perspective of the coupled propulsion discipline.

Data Availability Statement

The data used to support the findings of this study are available from the corresponding author upon request.

Conflicts of Interest

The authors declare no conflicts of interest.

Funding

This study is supported by the National Natural Science Foundation of China (Grant No. U20B2007).

Acknowledgments

This study is supported by the National Natural Science Foundation of China (Grant No. U20B2007). All authors would like to thank them.

References

[1] G. N. Kumar, D. Penchalaiah, A. K. Sarkar, and S. E. Talole, "Hypersonic boost glide vehicle trajectory optimization using genetic algorithm," *IFAC-Papers OnLine*, vol. 51, no. 1, pp. 118–123, 2018.

[2] X. Zhou, R. He, H. B. Zhang, G. J. Tang, and W. M. Bao, "Sequential convex programming method using adaptive

mesh refinement for entry trajectory planning problem," *Aerospace Science and Technology*, vol. 109, article 106374, 2021.

[3] P. Dai, D. Z. Feng, W. H. Feng, J. S. Shan, and L. H. Zhang, "Entry trajectory optimization for hypersonic vehicles based on convex programming and neural network," *Aerospace Science and Technology*, vol. 137, article 108259, 2023.

[4] Z. B. Wang and Y. Lu, "Improved sequential convex programming algorithms for entry trajectory optimization," *Journal of Spacecraft and Rockets*, vol. 57, no. 6, pp. 1373–1386, 2020.

[5] K. Sachan and R. Padhi, "A brief survey on six-degree-of-freedom modeling for air-breathing hypersonic vehicles," *IFAC-PapersOnLine*, vol. 51, no. 1, pp. 492–497, 2018.

[6] Y. K. Ding, X. K. Yue, G. S. Chen, and J. S. Si, "Review of control and guidance technology on hypersonic vehicle," *Chinese Journal of Aeronautics*, vol. 35, no. 7, pp. 1–18, 2022.

[7] Z. Jiang and R. Zhou, "Particle swarm optimization applied to hypersonic reentry trajectories," *Chinese Journal of Aeronautics*, vol. 28, no. 3, pp. 822–831, 2015.

[8] X. F. Liu, P. Lu, and B. F. Pan, "Survey of convex optimization for aerospace applications," *Astrodynamics*, vol. 1, no. 1, pp. 23–40, 2017.

[9] T. R. Jorris and R. G. Cobb, "Three-dimensional trajectory optimization satisfying waypoint and no-fly zone constraints," *Journal of Guidance, Control, and Dynamics*, vol. 32, no. 2, pp. 551–572, 2009.

[10] J. M. Acton, "Hypersonic boost-glide weapons," *Science & Global Security*, vol. 23, no. 3, pp. 191–219, 2015.

[11] H. Y. Zhou, X. G. Wang, and N. G. Cui, "Glide trajectory optimization for hypersonic vehicles via dynamic pressure control," *Acta Astronautica*, vol. 164, pp. 376–386, 2019.

[12] Y. H. Luo, C. Xu, A. H. Zhao, Z. Yu, and J. Y. Wang, "A method of trajectory optimization design for rocket-powered hypersonic vehicle," *Mechanics in Engineering*, vol. 44, no. 6, pp. 1303–1312, 2022.

[13] J. Lin, Y. Z. He, and P. X. Huang, "Powered hypersonic vehicle reentry trajectory optimization based on improved multiphase Gauss spectral method," *Control Theory & Applications*, vol. 36, no. 10, pp. 1662–1671, 2019.

[14] J. Lin, Y. Z. He, and P. X. Huang, "Research on reentry trajectory of powered hypersonic vehicle with discontinuous ignition," *Acta Armamentarh*, vol. 41, no. 7, pp. 1307–1316, 2020.

[15] D. Chai, Y. W. Fang, Y. L. Wu, and S. H. Xu, "Boost-skipping trajectory optimization for air-breathing hypersonic missile," *Aerospace Science and Technology*, vol. 46, pp. 506–513, 2015.

[16] Y. Feng, R. S. Wan, Y. X. Mei, H. F. Sun, and L. N. Wu, "Reentry trajectory planning for range-extended hypersonic vehicles with boosters," *Journal of Beijing University of Aeronautics and Astronautics*, vol. 46, no. 8, pp. 1503–1513, 2020.

[17] J. Lin, Y. Z. He, and Z. Wang, "Reentry trajectory optimization of powered hypersonic vehicle for improving range based on discontinuous ignition," in *2020 Chinese Automation Congress (CAC)*, pp. 4445–4450, Shanghai, China, 2020.

[18] T. T. Zhang, X. T. Yan, W. Huang, X. K. Che, and Z. G. Wang, "Multidisciplinary design optimization of a wide speed range vehicle with waveride airframe and RBCC engine," *Energy*, vol. 235, article 121386, 2021.

[19] Z. G. Wu and Y. B. Liu, "Integrated optimization design using improved pigeon-inspired algorithm for a hypersonic vehicle model," *International Journal of Aeronautical and Space Sciences*, vol. 23, no. 5, pp. 1033–1042, 2022.

[20] J. Sobieszczanski-Sobieski, "A linear decomposition method for large optimization problems. Blueprint for development," NASA Technical Memorandum, 1982.

[21] A. A. Giunta, O. Golividov, D. L. Knill, B. Grossman, W. H. Mason, and L. T. Watson, "Multidisciplinary design optimization of advanced aircraft configurations," in *Fifteenth International Conference on Numerical Methods in Fluid Dynamics: Proceedings of the Conference Held in Monterey, CA, USA, 24–28 June 1996*, pp. 14–34, Springer, Berlin Heidelberg, 1997.

[22] J. R. Olds, "Multidisciplinary design techniques applied to conceptual aerospace vehicle design," North Carolina State University, 1993.

[23] A. Viviani, A. Aprovitola, L. Iuspa, and G. Pezzella, "Aeroshape design of reusable re-entry vehicles by multidisciplinary optimization and computational fluid dynamics," *Aerospace Science and Technology*, vol. 105, article 106029, 2020.

[24] H. Yan and X. B. Zhang, "A self-adaptive local diversity-preserving NSGA-II for the multidisciplinary design optimization of a miniaturized supersonic rocket," *Aerospace Science and Technology*, vol. 136, article 108230, 2023.

[25] A. Benaouali and S. Kachel, "Multidisciplinary design optimization of aircraft wing using commercial software integration," *Aerospace Science and Technology*, vol. 92, pp. 766–776, 2019.

[26] D. Zhang, S. Tang, and J. Che, "Concurrent subspace design optimization and analysis of hypersonic vehicles based on response surface models," *Aerospace Science and Technology*, vol. 42, pp. 39–49, 2015.

[27] H. P. Zhen and C. W. Jiang, "Overview of the hypersonic technology validation vehicle HTV-2," *Aerodynamic Missile Journal*, vol. 6, pp. 7–13, 2013.

[28] Y. X. Yang, Y. S. Chen, H. H. Yang, and C. J. Wu, "Blunt method of lift body configuration and aerodynamic performance analysis," *Journal of Zhejiang University*, vol. 57, no. 6, pp. 1242–1250, 2023.

[29] Y. X. Yang, W. W. Zhao, Y. T. Xue, H. Yang, and C. J. Wu, "Improved automatic kernel construction for Gaussian process regression in small sample learning for predicting lift body aerodynamic performance," *Physics of Fluids*, vol. 35, no. 6, article 066108, 2023.

[30] Z. Z. Guo, Z. Q. He, C. C. Xia, and W. F. Chen, "KD tree method for efficient wall distance computation of mesh," *Journal of National University of Defense Technology*, vol. 39, no. 4, pp. 21–25, 2017.

[31] Z. Z. Guo, Z. Q. He, W. W. Zhao, and W. F. Chen, "Efficient mesh deformation and flowfield interpolation method for unstructured mesh," *Acta Aeronautica et Astronautica Sinica*, vol. 39, no. 12, pp. 133–144, 2018.

[32] Q. Miao, Z. B. Shen, H. H. Zhang, and H. T. Sun, "Multiobjective optimization method of solid rocket motor finocyl grain based on surrogate model," *Aerospace*, vol. 9, no. 11, p. 679, 2022.

[33] Z. P. Wu, D. H. Wang, F. Hu, and W. H. Zhang, "Surrogate based grain design optimization for solid rocket motor," *Journal of Solid Rocket Technology*, vol. 39, pp. 321–326, 2016.

[34] W. F. Fan, B. Xu, and J. Hao, "Multidisciplinary design optimization for boost-glide vehicle overall design," *Modern Defense Technology*, vol. 43, no. 1, pp. 46–51, 2015.

[35] C. L. Darby, W. W. Hager, and A. V. Rao, "An hp-adaptive pseudospectral method for solving optimal control problems,"

Optimal Control Applications and Methods, vol. 32, no. 4, pp. 476–502, 2011.

[36] G. T. Huntington, "Advancement and analysis of a Gauss pseudospectral transcription for optimal control problems," Massachusetts Institute of Technology, Department of Aeronautics and Astronautics, 2007.

[37] M. E. Tauber, "A review of high-speed, convective, heat-transfer computation methods," in *NASA-TP-2914*, USA NASA, Hampton, Virgi-na, 1989.

[38] Y. G. Zhang, K. L. Song, D. H. Liu, C. Y. Xiong, and S. A. Chou, "A multi-mode failure boundary exploration and exploitation framework using adaptive kriging model for system reliability assessment," *Probabilistic Engineering Mechanics*, vol. 73, article 103473, 2023.

[39] C. He, R. P. Liu, and Z. W. He, "Seismic vulnerability assessment on porcelain electrical equipment based on kriging model," *Structure*, vol. 55, pp. 1692–1703, 2023.

[40] H. J. Chu, Y. P. Lin, C. S. Jang, and T. K. Chang, "Delineating the hazard zone of multiple soil pollutants by multivariate indicator kriging and conditioned Latin hypercube sampling," *Geoderma*, vol. 158, no. 3-4, pp. 242–251, 2010.

[41] F. Tu, M. Bhat, P. Blondin, P. Vincent, M. Sharafi, and J. D. Benson, "Machine learning and hypothesis driven optimization of bull semen cryopreservation media," *Scientific Reports*, vol. 12, no. 1, p. 22328, 2022.